Biosensors and Bioelectronics 72 (2015) 168–174

Contents lists available at ScienceDirect

Biosensors and Bioelectronics

journal homepage: www.elsevier.com/locate/bios

Towards intrinsic graphene biosensor: A label-free, suspended single crystalline graphene sensor for multiplex lung cancer tumor markers detection

Peng Li [a,b], Bo Zhang [b], Tianhong Cui [b,*]

[a] State Key Laboratory of Precision Measurement Technology and Instruments, Department of Precision Instruments, Tsinghua University, Beijing 100084, China

[b] Department of Mechanical Engineering, University of Minnesota, Minneapolis, MN 55455, USA

ARTICLE INFO

Article history:
Received 30 April 2015
Accepted 5 May 2015
Available online 7 May 2015

Keywords:
Graphene
Single crystalline
Suspended beam
Cancer sensor
Label-free

ABSTRACT

Graphene biosensors reported so far are based on polycrystalline graphene flakes which are anchored on supporting substrates. The influence of grain boundary and the scattering from substrate drastically degrade the properties of graphene and conceal the performance of intrinsic graphene as a sensor. Here we report a label-free biosensor based on suspended single crystalline graphene (SCG), which can get rid of grain boundary and substrate scattering, revealing the biosensing mechanism of intrinsic graphene for the first time. Monolayer SCG flakes were derived from low pressure chemical vapor deposition (LPCVD) method. Multiplex detection of three different lung cancer tumor markers was realized. The suspended structure can largely improve the sensitivity and detection limit (0.1 pg/ml) of the sensor, and the single crystalline nature of SCG enable the biosensor to have superior uniformity compared to polycrystalline ones. The SCG sensors exhibit superb specificity and large linear detection range from 1 pg/ml to 1 μg/ml, showing the prominent advantages of graphene as a sensing material.

1. Introduction

Tumor markers are small biological molecules in human's blood and tissue, and their high level of concentrations indicate certain cancers are very likely present inside the human body (Zhong et al., 2010). Therefore, tumor marker detection is very critical in disease prediction, diagnosis, and cancer treatment monitoring. The clinical utility of tumor marker to discriminate health and disease requires the capability to measure extremely low concentration protein biomarkers, which is also important to understand cellular processes and to search for new protein biomarkers (Mohammed and Desmulliez, 2014). Conventional techniques, such as enzyme linked immunosorbent assay (ELISA) (Sato et al., 2014), surface plasmon resonance (SPR) (Liang et al., 2012), and magnetic beads detection (Chang et al., 2006), have been widely used for detecting tumor markers. However, the detection limits of these methods have lagged behind the requirements for clinical utility and research. Additionally, these techniques require time-consuming target-labeling process, such as fluorescent dyes and quantum dots labeling (Petryayeva et al., 2013), or sophisticated optical detection system. These drawbacks limit the clinical application of tumor marker detection.

Graphene is an attractive material for label-free detecting tumor markers in clinical applications and research, which can overcome the hurdles of the previous detection methods. Graphene, a two-dimensional honeycomb crystal of sp^2-bonded carbon atoms (Novoselov et al., 2004), has drawn significant attention in both fundamental and applied research fields, owing to its extraordinary electrical, mechanical, and chemical properties. Graphene's extremely high carrier mobility (Du et al., 2008), thermal conductivity (Balandin et al., 2008), Young's modulus (Lee et al., 2008, 2012), breaking strength (Lee et al., 2013; Rasool et al., 2013), and extremely low noise (Robinson et al., 2008) make it an excellent candidate for nanoelectromechanical systems (NEMS) sensors and actuators (Bunch et al., 2007; Chen et al., 2009; Gomez-Navarro et al., 2008; Chen C. et al., 2013). Graphene based label-free biosensors hold the great potential to have superb performances with low cost (suitable for long term dynamic monitoring) (Zhang et al., 2012). They are able to detect many types of molecules and ions in very low concentration situations by

* Corresponding author.
E-mail address: tcui@me.umn.edu (T. Cui).

http://dx.doi.org/10.1016/j.bios.2015.05.007
0956-5663/

monitoring the resistance shift caused by the adsorption of target molecules.

The performances of the sensors largely rely on the quality of graphene film. Several techniques have been developed for producing high-quality graphene films, including mechanical cleavage from graphite (Liang et al., 2007; Song et al., 2009), decomposition of SiC (Shivaraman et al., 2009), and chemical vapor deposition (CVD) growth on metallic surfaces such as copper (Li et al., 2009; van der Zande et al., 2010; Yu et al., 2011), nickel (Kim et al., 2009;), and platinum (Gao et al., 2012). CVD with copper substrate has the ability for the growth of large-area monolayer graphene with relatively low cost, attracting increasing attention recently. During growth, graphene grains initially nucleate from random locations. Then the growth of such grains proceeds, and these grains eventually form a polycrystalline film. Therefore, sensors based on large area graphene film reported so far are polycrystalline (Jin et al., 2014; Her et al., 2013). The grain boundaries degrade graphene material properties drastically, thus lead to deterioration on device's performance (Milaninia et al., 2009). The performances of polycrystalline graphene biosensors show large deviation from device to device (Yue et al., 2014), which reason has not been investigated so far. It has become the hurdle of their practical application. Additionally, the research has been focused on graphene sensors anchored on supporting substrates (Yue et al., 2014; Zheng et al., 2005; Xu et al., 2014). Carrier scattering from the substrate largely reduces the carrier mobility of the film, drastically affecting the performance of the sensor. Therefore, the influence of grain boundary and the scattering from substrate deteriorate the properties of graphene and the performance of biosensor based on it.

Here we report a label-free biosensor based on suspended single crystalline graphene, which can get rid of grain boundary and substrate scattering, revealing the sensing mechanism of intrinsic graphene. The SCGs were derived from LPCVD by controlling the growth duration. Multiplex detection of lung cancer biomarkers with easy operation was realized. The lung cancer sensors are ultra-sensitive due to free-standing structure, and they show improved uniformity because of the single-crystalline nature of the film.

2. Experiments

2.1. Materials

0.1% Poly-L-lysine (PLL) was received from Sigma-Aldrich Inc. without further treatments. 3% Bovine serum albumin (BSA) was purchased from Sigma-Aldrich Inc. Three types of lung cancer bio markers, ANXA2, ENO1, and VEGF (both antibody and antigen), were purchased from Sigma-Aldrich Inc. The copper foil (25 μm thick, 99.8%, Product no. 046365) was received from Alfa Aesar.

2.2. LPCVD SCG synthesis

The LPCVD graphene growth was carried out in a 2 inch quartz tube furnace on polycrystalline copper substrates with a mixture of research grade methane (as the carbon source) and hydrogen. Before growth, the as-received copper foil was pre-treated by 1:10 diluted nitric acid to remove the native copper oxide for a better growth of graphene, since the oxide could degrade the catalytic ability of copper. Copper foil was quickly loaded into CVD furnace and pumped down to base pressure (< 5 mTorr). Then the furnace was heated up to 1050 °C under 10 SCCM hydrogen. After reaching 1050 °C, the sample was annealed for 30 min or longer, which can

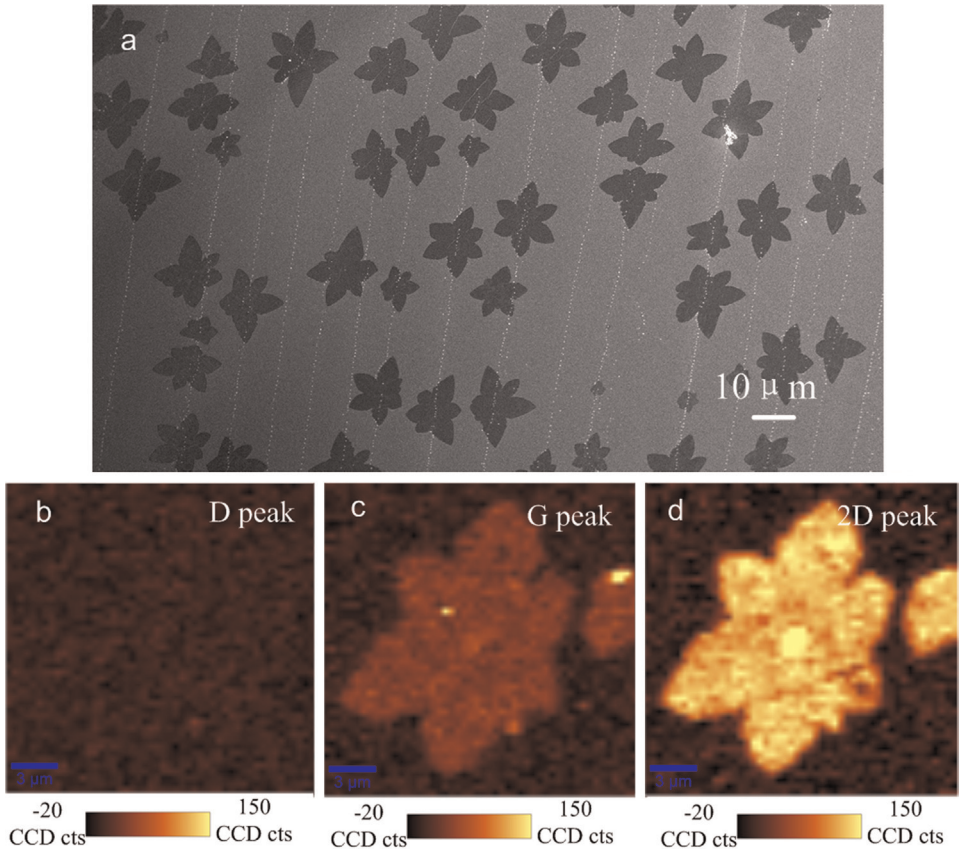

Fig. 1. CVD growth of SCG. (a) SEM image of LPCVD growth of SCGs on copper foil. (b) Raman D peak intensity image of a SCG which shows negligibly small D peak intensity within SCG grain, indicating low defect of the film. (c) Raman G peak intensity image of the same SCG. (d) Raman 2D peak intensity image of the same SCG.

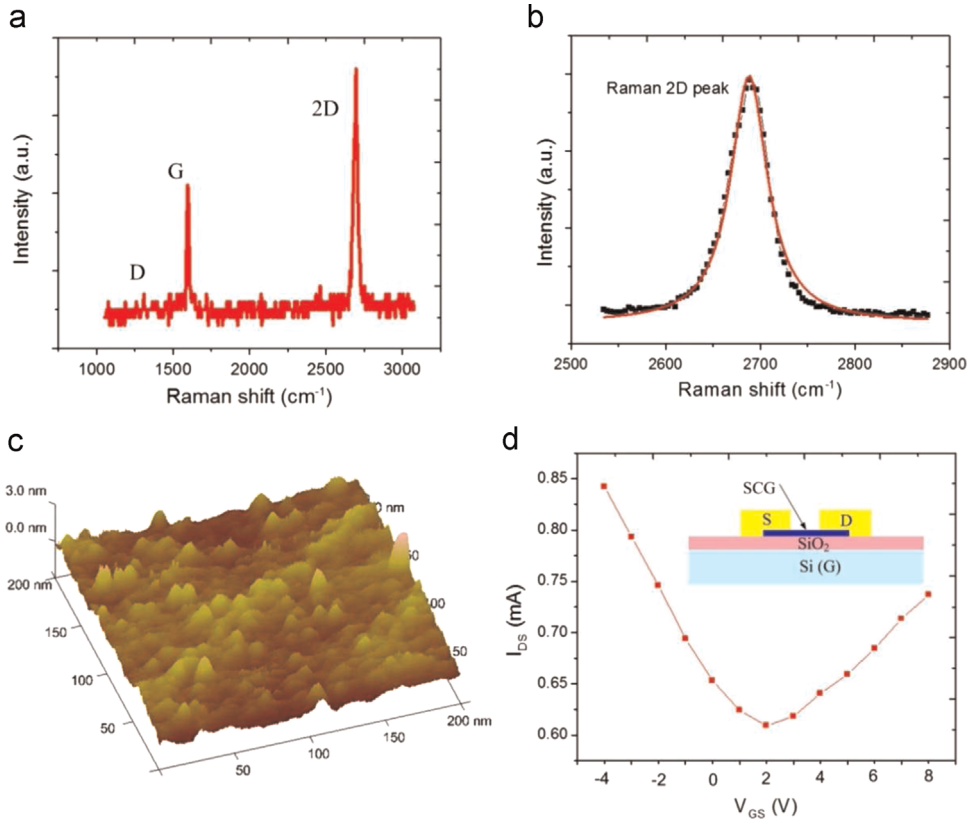

Fig. 2. SCG characterization. (a) A typical Raman spectrum of SCG. (b) Raman 2D peak curve (black dots) and Lorentzian fitting for 2D peak (red line). 2D peak of a monolayer graphene can be fitted by a single Lorentzian. (c) AFM topographic image of monolayer SCG on SiO_2 surface. The roughness of SCG is 210 pm. (d) I_{DS} vs V_{GS} of a SCG FET. The gate can cause either electron or hole conduction with transition point at $V_{GS}=2$ V. The inset is a schematic view of SCG FET. (For interpretation of the references to color in this figure legend, the reader is referred to the web version of this article.)

further strip the copper oxide. The growth was then carried out under a gas mixture of 0.6 SCCM methane and 10 SCCM hydrogen. Finally, the sample was rapidly cooled to room temperature without changing the gas flow rate. Because grain boundaries of a continuous polycrystalline graphene film is hardly visible even under scanning electron microscope (SEM), the growth duration was controlled before isolated SCG islands connected to each other to avoid grain boundary during device fabrication. Most of monolayer SCG islands derived from LPCVD have six-lobed shapes and are distributed across the copper foil (Fig. 1a). Decreasing methane flow rate reduces the nucleation density effectively, thus larger grain size. With appropriate growth parameters, each SCG grain can easily reach tens of micrometers, large enough to fabricate single or multiple devices. After LPCVD growth, SCGs was transferred from copper foil onto a Si substrate with 300 nm SiO_2 on top by PMMA (polymethyl methacrylate) assisted process similar to those reported previously (van der Zande et al., 2010). The sample was heated up to 300 °C at low pressure for 3 h to remove PMMA residues which may affect the properties of intrinsic graphene (Cheng et al., 2011).

2.3. Sensor fabrication

Free-standing SCG sensors were fabricated with micro-manufacture processes. The electrodes were defined by photolithography, followed by image reverse technique, Cr (10 nm)/Au (100 nm) electron-beam evaporation, and metal lift-off. One of the six-lobed shaped monolayer SCGs was chosen and etched into rectangular beams by O_2 plasma dry etching. We designed graphene nuclei located beneath contact electrodes instead of on the beam, because graphene nuclei may have relatively more defects than other parts of graphene. 1:10 BOE (buffered oxidize etcher) was applied to etch SiO_2 beneath graphene and release the free-standing structure, followed by critical point drying to avoid stiction. We fabricated SCG beams with lengths range from 2 to 5 μm. The width of the beam is about 2 μm.

3. Results and discussion

3.1. SCG characterization

SCG's quality was characterized by a Witec Alpha300R Confocal Raman microscope with excitation laser wavelength of 514 nm and the power of the laser below 6 mW to avoid sample damage. The intensities of detected graphene Raman peaks, D ($\sim$1350 cm^{-1}), G ($\sim$1580 cm^{-1}) and 2D ($\sim$2680 cm^{-1}) were extracted and their distributions (Raman mappings) are plotted in Fig. 1b–d for a single SCG grain (the Raman mappings are 60×60 pixels, and each pixel has 0.3 s accumulation time). Negligibly small D peak over most of the area within a graphene grain was observed in Figs. 1b and 2a, indicating good quality and single-crystal nature of our sample, since grain boundary defect could cause prominent D peak in Raman spectrum. Fig. 2a shows typical features of monolayer graphene: a symmetric 2D band centered at $\sim$2680 cm^{-1}, and $\sim$0.5 G to 2D intensity ratio. Lorentzian fitting of 2D peak further proofs the monolayer nature of SCG (Fig. 2b), because 2D peak curve of a monolayer graphene can be fitted by a single Lorentzian peak, while a bi-layer requires four Lorentzians. Atomic force microscope (AFM) topographic image of SCG on SiO_2 surface demonstrates the roughness of 210 pm (Fig. 2c), close to the roughness of monolayer graphene measured by Koenig et al.

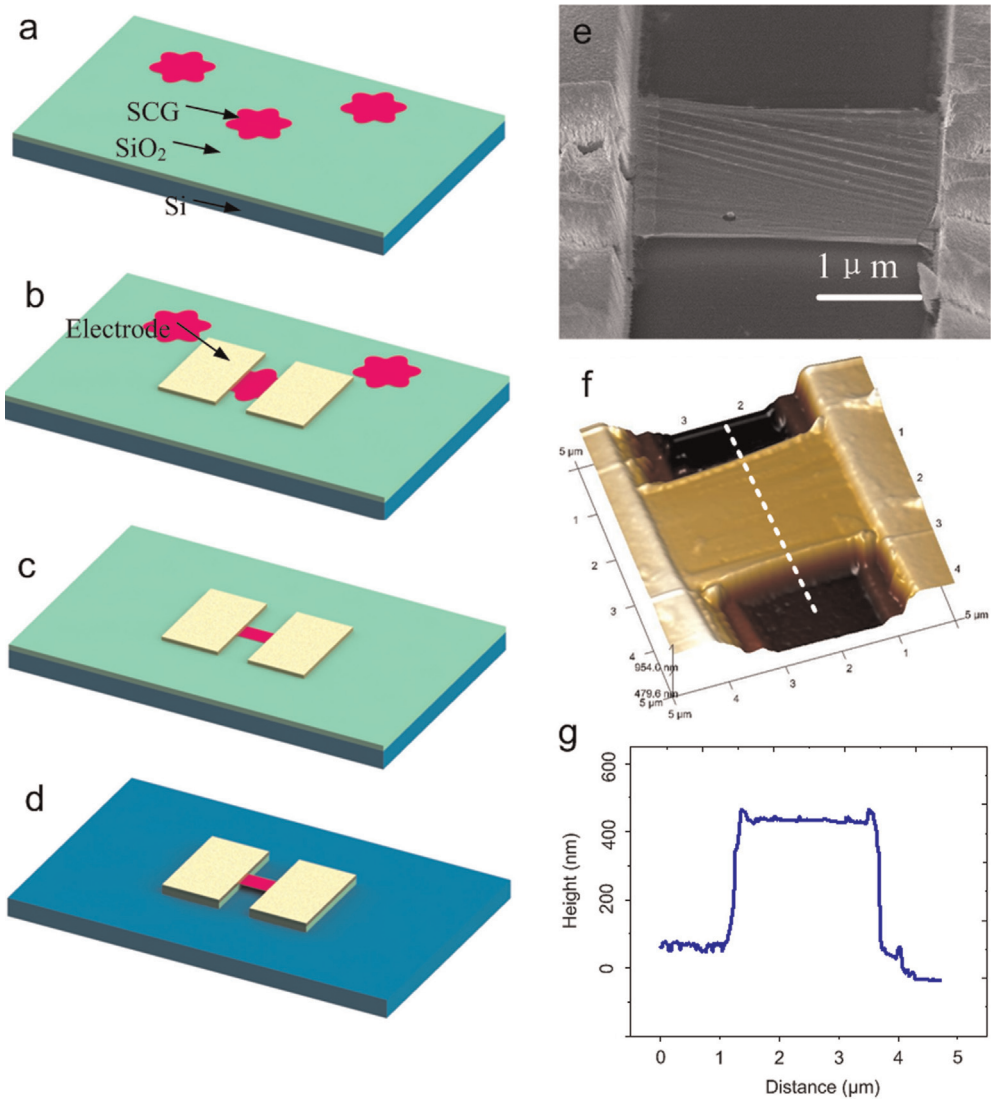

Fig. 3. SCG sensor fabrication. (a–d) SCG sensor fabrication process. (a) Transfer SCGs from copper foil onto SiO_2/Si substrate by PMMA assisted process. (b) Choose a SCG and fabricate metal electrodes on it. (c) Etch SCG into rectangular beam shape. (d) Etch SiO_2 beneath to release the suspended SCG beam. (e) SEM image of a suspended SCG beam. (f) AFM topographic image of a SCG beam. (g) The AFM line scan of SCG beam marked with white dot line in f. It proves that the SCG is suspended and the distance between the beam and substrate is about 300 nm.

(2011).

Measuring carrier mobility is another common way to evaluate material quality. SCG field effect transistors (FETs) were fabricated on a silicon substrate with a top gate thermal oxide layer. The I_{DS} versus V_{GS} curve shows electron/hole conduction shifted at a transition point (Dirac point) of V_{GS}=2 V (Fig. 2d). The slightly shift of Dirac point could be caused by PMMA residue during transfer process (Cheng et al., 2011) or water molecules (Novoselov et al., 2004). Carrier mobility of graphene can be deduced from (Liang et al., 2007)

$$\mu = \frac{\Delta I_{DS}}{C_{OX}\frac{W}{L}V_{DS}\,\Delta V_{GS}} \tag{1}$$

where L and W are FET length and width, respectively, $C_{OX} = \varepsilon_{OX}\,\varepsilon_0 t_{OX}$ is gate oxide capacitance (ε_{OX} =3.9 is silicon dioxide permittivity, ε_0 is vacuum permittivity, and t_{OX} is gate oxide thickness). The carrier mobility of 6300 $cm^2V^{-1}s^{-1}$ is deduced under ambient conditions. This high carrier mobility is comparable to or even larger than that of SCG from regular CVD growth reported in literature, ~5200 $cm^2V^{-1}s^{-1}$ (Chen C. et al., 2013), indicating the superb quality of our SCG. We believe the carrier mobility of SCG could be even larger by using boron nitride substrates (Dean et al., 2010) or suspended structure to reduce the charge impurities trapped in SiO_2.

3.2. SCG sensor characterization

Fig. 3e and f are SEM and AFM images of a SCG sensor, respectively. The SEM image clearly demonstrates the suspension of SCG. AFM line scan curve in Fig. 3g indicates that the width of the beam is about 2 μm, and the gap between SCG and substrate is close to 300 nm, which is the thickness of SiO_2 sacrificial layer.

The free-standing SCG was immersed into 0.1% PLL aqueous solution positive charged for 2 h, enhancing the immobilization of antibodies. Then the sensor was incubated for overnight at 4 °C in capture antibody solution at a concentration of 6 μg/ml. Sequentially, it was incubated in a 3% BSA blocking solution at room temperature for 5 h to block nonspecific binding sites. After the immobilization process, the label-free suspended SCG sensor was ready for detection. ANXA2, VEGF, and ENO1 are important lung cancer biomarkers (Yang et al., 2015; Yu et al., 2014; Schwaedrle

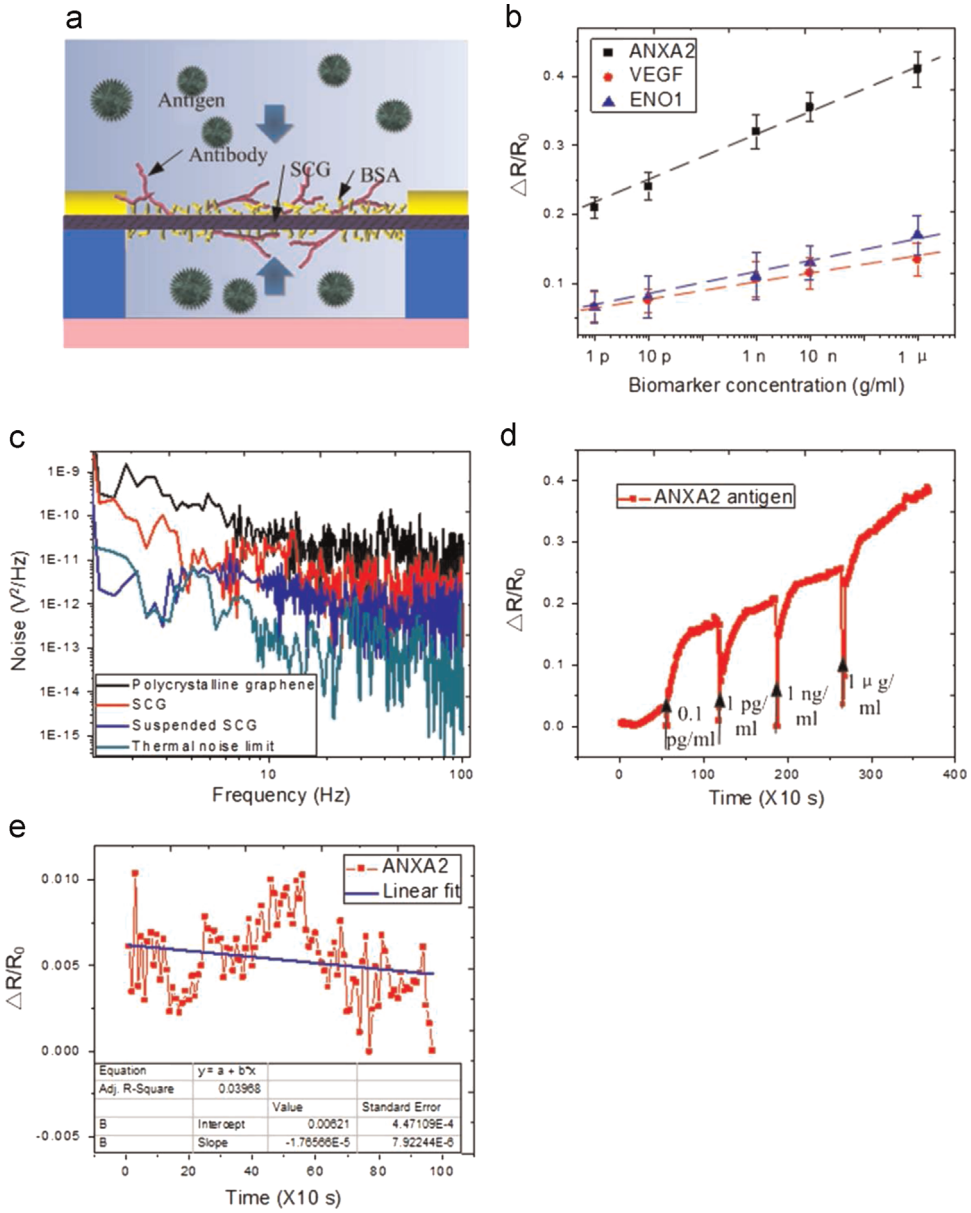

Fig. 4. (a) Schematic illustration of immunoreaction of suspended SCG biosensor. (b) The SCG sensor's response to 3 different types of lung cancer tumor markers. Tumor markers with higher concentration result in larger resistance shift of the sensor. (c) Comparison of low-frequency noise in polycrystalline graphene, non suspended SCG and suspended SCG. Suspended SCG has the smallest low-frequency noise. (d) Resistance shift versus time curve of SCG sensor, which is capable of detecting 0.1 pg/ml ANXA2. (e) Noise of SCG biosensor during ANXA2 detection, which is 4.47×10^{-4} $\Delta R/R_0$.

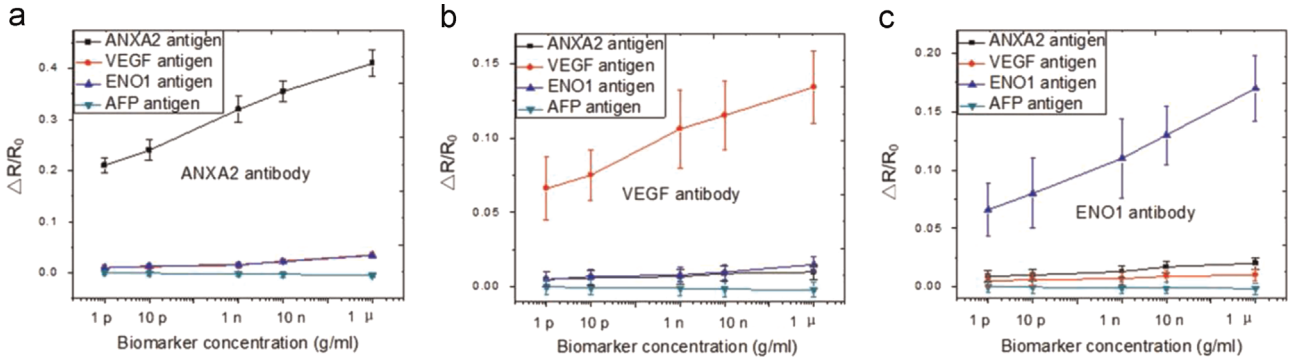

Fig. 5. Specificity of SCG sensor. (a) SCG sensors with ANXA2 antibody only have prominent response to ANXA2 antigen. (b) SCG sensors with VEGF antibody only have prominent response to VEGF antigen. (c) SCG sensors with ENO1 antibody only have prominent response to ENO1 antigen.

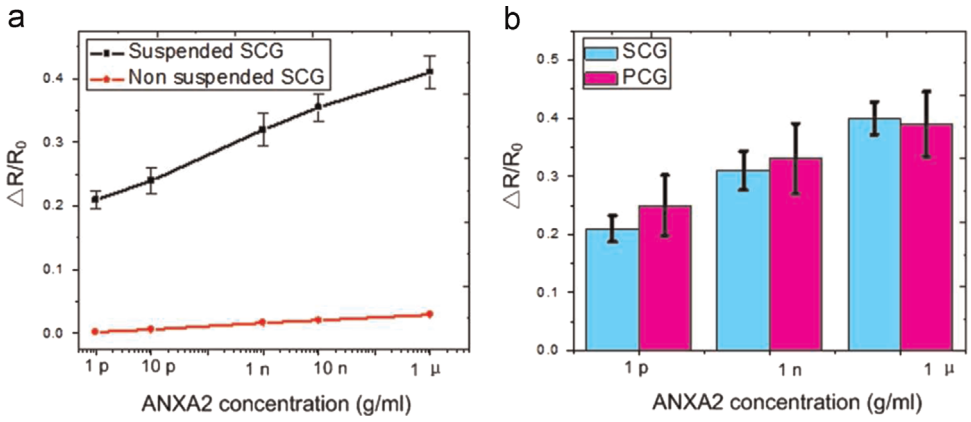

Fig. 6. (a) Comparison of suspended and non-suspended SCG sensors. Suspended SCG sensor with less influence from substrate has much better sensitivity. (b) Comparison of SCG, and PCG sensors resistance shift caused by ANXA2 antigen with different concentration. SCG sensors have smaller error bar (standard deviation of $\Delta R/R_0$) because of its single crystalline nature, indicating better uniformity.

et al., 2015). SCG biosensors for lung cancer early prognosis were functionalized by immobilizing antibody of these three tumor markers on different graphene beams. This label-free lung cancer biosensor was characterized by measuring SCG resistance shift according to different concentrations of lung cancer biomarker using Agilent Data Logger (34970 A, Agilent Inc.). It is low cost and easy to operate. Due to the stickiness of water and surface force in micro-scale, all of our immobilization and detection experiments were processed in solution to avoid the collapse of suspended SCG beam structure.

Fig. 4b, shows the response of SCG sensors to three types of lung cancer tumor markers, ANXA2, VEGF, and ENO1 with different concentrations. Tumor markers with higher concentration results in larger resistance shift of the sensor, and all the curves show good linear response from 1 pg/ml to 1 μg/ml. The graphene biosensor's response can be explained by the strong interaction between antigen and its bio-receptors (Fig. 4a). It is evident that the absorption of molecules by the bio-receptors on the surface of graphene can cause the change in density and mobility of charge carriers of the film, resulting in different graphene resistance values. The equation, $\rho = (1/nq\mu)$, shows this relation clearly, where ρ is SCG resistance, n is carrier density, q is charge per carrier. The isoelectric point of ANXA2, VEGR, and ENO1 (7.55, 8.50, 7.01) are higher than pH value of antigen solution. As a result, antigen molecules are positively charged. When the gate voltage is 0, hole is the main carrier in graphene channel (Fig. 2d). Antigen molecules absorbed on graphene surface act as a positive gate voltage which repels holes, reducing carrier density n. Additionally, the scattering due to antigen molecules reduces the carrier mobility μ, which further decreases the conductivity of graphene.

One significant consideration for NEMS sensor is the low-frequency noise (dominated by 1/f noise), because the detection limit of a sensor is ultimately determined by its signal-to-noise ratio. Thus the noise spectra of single crystalline and polycrystalline graphene were investigated and compared under the same experimental conditions. The low frequency noise in SCG is approximately 1 folder smaller than that in polycrystalline graphene devices (Fig. 4c). Without the scattering from the substrate, the free-standing SCG shows 1 folder smaller low-frequency noise than that in SCG anchored on SiO_2 substrate, approximately. These two factors contribute to the superb detection limit of our suspended SCG sensor. The detection limit is generally defined as three times the standard deviation of the noise (Pretsch, 2007). The output signal $\Delta R/R_0$ of our sensor for 0.1 pg/ml ANXA2 antigen (Fig. 4d) is larger than three times the standard deviation of noise (4.47×10^{-4} $\Delta R/R_0$) (Fig. 4e). Therefore, bio-sensor based on the suspended SCG can reach very low concentration of 0.1 pg/ml. On the other hand, the detection limit of most graphene biosensors reported are not lower than 1 pg/ml (Huang et al., 2015; Wang et al., 2014; Teixeira et al., 2013; Jin et al., 2014), and the detection limit of ANXA2, VEGF, and ENO1 reported are higher than 2 pg/ml (Yang et al., 2015; Ho et al., 2010; Lin et al., 2015; Semeraro et al., 2014). Fig. 4d demonstrates that SCG sensors can response to the existence of target tumor marker within only a few minutes.

Specificity is critical for biosensors to identify each type of tumor marker correctly and reduce the chance of misleading. Eight SCG sensors immobilized with ANXA2 antibody were put into ANXA2, VEGF, ENO1 and AFP (alpha-fetoprotein) solution, respectively. The sensor's response to ANXA2 antigen is 1 order larger than that to other molecules (Fig. 5a). Similar results were observed for sensors with VEGF or ENO1 antibody (Fig. 5b, c). The good specificity of SCG sensor is not only based on the specific binding performance between antigen and corresponding antigen. Importantly, the nonspecific binding sites on graphene surface were blocked by BSA, which further avoid the absorption of non specific molecules. These results also prove that the resistance change of our sensor was caused by the molecular interaction instead of other factors in environment.

3.3. Biomarker detection by non-suspended graphene

Electronic measurements of 8 suspended SCG cancer sensors demonstrate their improved sensitivity compared to 8 non-suspended ones manufactured and tested under the same conditions (Fig. 6a). Carrier mobility plays an important role in bio-sensing, and higher carrier mobility is related to better sensitivity. The charge impurities trapped in SiO_2 drastically reduce the carrier mobility of the SCG film anchored on substrate surface, while free-standing SCG can get rid of this negative influence (Carrier mobility of free-standing graphene is 6 times larger) (Du et al., 2008). Besides, both sides of the free-standing SCG beam were immobilized with bio-receptors which can absorb more target biomarkers, providing larger sensing area and better sensitivity.

3.4. Biomarker detection by polycrystalline graphene

In order to investigate the uniformity of graphene sensor, polycrystalline graphene (PCG) sensors were fabricated and tested as well. Eight SCG and PCG sensors with the same geometry size were tested. The detection results demonstrate that the resistance shift value of SCG sensors has smaller standard deviation ($< 50\%$ of that of PCG), indicating better uniformity (Fig. 6b). According to Yu et al. (2011), the resistance across graphene grain boundary is

about 1 order larger than that of graphene. Normal resistance of our SCG device is 200–400 Ω, while it is 1–3 kΩ for PCG. Therefore, the properties of graphene are overwhelmed by grain boundary in PCG sensors, and it was actually the response of the grain boundary instead of graphene itself that was detected during bio-sensing. Although grain boundary could enhance the sensitivity of the sensor (Yasaei et al., 2014), different grain boundaries show very different electrical properties (symmetric grain boundary provides much less reflection to carriers than asymmetric grain boundary does (Yazyev and Louie, 2010)). Besides, grain boundaries in different PCG may have various locations and orientations, which further contribute to the large deviation of the performance between PCG devices. On the other hand, SCGs have identical nano-structure, resulting superior uniformity. Additionally, SCG beams are much less likely to break down during detection without the mechanically weak grain boundary.

4. Conclusion

Label-free SCG biosensor was demonstrated for the first time, and three kinds of tumor markers related to lung cancer diagnosis were detected with easy operational process. The suspended structure, which has better carrier mobility, sensing area, and low frequency noise, are responsible for enhanced sensitivity and superb detection limit (0.1 pg/ml) of the sensors. The SCG sensors exhibit good specificity and large linear detection range from 1 pg/ml to 1 μg/ml. The single crystalline nature of SCG enables the devices to have better uniformity than other biosensors based on graphene. This work shows the prominent advantages of intrinsic graphene as a sensing material.

Acknowledgment

The work described in this paper was supported in part by the National Natural Science Foundation of China (No. 51405257) and Science Fund of China Post Doctor (No. 2012M520259). The authors acknowledge the assistance of fabrication and characterization from Minnesota Nano Center and Characterization Facility at the University of Minnesota.

References

Balandin, A.A., Ghosh, S., Bao, W., Calizo, I., Teweldebrhan, D., Miao, F., Lau, C.N., 2008. Nano Lett. 8, 902–907.
Bunch, J.C., vander Zande, A.M., Verbridge, S.S., Frank, I.W., Tanenbaum, D.M., Parpia, J.M., Craighead, H.G., McEuen, P.L., 2007. Science 315, 490–493.
Chang, T.L., Tsai, C.Y., Sun, C.C., Uppala, R., Chen, C.C., Lin, C.H., Chen, P.H., 2006. Microelectron. Eng. 83, 1630–1633.
Chen, C., Rosenbatt, S., Bolotin, K.I., Kalb, W., Kim, P., Kymissis, I., Stormer, H.L., Heinz, T.F., Hone, J., 2009. Nat. Nanotechnol. 4, 861–867.
Chen, C., Lee, S., Deshpande, V.V., Lee, G.H., Lekas, M., Shepard, K., Hone, J., 2013. Nat. Nanotechnol. 8, 923–927.
Cheng, Z., Zhou, Q., Wang, C., Li, Q., Wang, C., Fang, Y., 2011. Nano Lett., 767–771.
Du, X., Skachko, I., Barker, A., Andrei, E.Y., 2008. Nat. Nanotechnol. 3, 491–495.
Dean, C.R., Young, A.F., Lee, M.C., Sorgenfrei, S., Watanabe, K., Taniguchi, T., Kim, P., Shepard, K.L., Hone, J., 2010. Nat. Nanotechnol. 5, 722.
Gao, L., Ren, W., Xu, H., Jin, L., Wang, Z., Ma, T., Ma, L.P., Zhang, Z., Fu, Q., Peng, L.M., Bao, X., Cheng, H.M., 2012. Nat. Commnun. 3, 699.
Gomez-Navarro, C., Burghard, M., Kern, K., 2008. Nano Lett. 8, 2045–2049.
Her, J.L., Pan, T.M., Lin, W.Y., Wang, K.S., Li, L.J., 2013. Sensor. Actuat. B-Chem. 182, 396–400.
Huang, J., Tian, J., Zhao, Y., Zhao, S., 2015. Sensor. Actuat. B-Chem. 206, 570–576.
Ho, J., Chang, H.C., Shih, N.Y., Wu, L.C., Chang, Y.F., Chen, C.C., Chou, C., 2010. Anal. Chem. 82, 5944–5950.
Jin, B., Wang, P., Mao, H., Hu, B., Zhang, H., Cheng, Z., Wu, Z., Bian, X., Jia, C., Jing, F., Jin, Q., Zhao, J., 2014. Biosens. Bioelectron. 55, 464–469.
Kim, K.S., Zhao, Y., Jang, H., Lee, S.Y., Kim, J.M., Kim, K.S., Ahn, J.H., Kim, P., Choi, J.Y., Hong, B.H., 2009. Nature 457, 706–710.
Koenig, S.P., Boddeti, N.G., Dunn, M.L., Bunch, J.S., 2011. Nat. Nanotechnol. 6, 543–546.
Liang, Y.H., Chang, C.C., Chen, C.C., Chu-Su, Y., Lin, C.W., 2012. Clin. Biochem. 45, 1689–1693.
Lee, C., Wei, X., Kysar, J.W., Hone, J., 2008. Science 321, 385–388.
Lee, G.H., Cooper, R.C., An, S.J., Lee, S., van der Zande, A., Petrone, N., Hammerberg, A.G., Lee, C., Crawford, Oliver, W., Kysar, J.W., Hone, J., 2013. Science 340, 1073–1076.
Lee, J.U., Yoon, D., Cheong, H., 2012. Nano Lett. 12, 4444–4448.
Liang, X., Fu, Z., Chou, S.Y., 2007. Nano Lett. 7, 3840–3844.
Li, X., Cai, W., An, J., Kim, S., Nah, J., Yang., D., Piner., R., Velamakanni, A., Jung, I., Tutuc, E., Banerjee, S.K., Colombo, L., Ruoff, R.S., 2009. Science 324, 1312–1314.
Lin, C.W., Wei, K.C., Liao, S.S., Huang, C.Y., Sun, C.L., Wu, P.J., Lu, Y.J., Yang, H.W., Ma, C.C.M., 2015. Biosens. Bioelectron. 67, 431–437.
Mohammed, M.I., Desmulliez, M.P.Y., 2014. Biosens. Bioelectron. 61, 478–484.
Milaninia, K.M., Baldo, M.A., Reina, A., Kong, J., 2009. Appl. Phys. Lett. 95, 183105.
Novoselov, K.S., Geim, A.K., Morozov, S.V., Jiang, D., Zhang, Y., Dubono, S.V., Grigorieva, I.V., Firsov, A.A., 2004. Science 306, 666–669.
Petryayeva, E., Algar, W.R., Medintz, I.L., 2013. Appl. Spectrosc. 67, 215–252.
Pretsch, E., 2007. TrAC–Trends Anal. Chem. 26, 46–51.
Rasool, H.I., Ophus, C., Klug, W.S., Zettl, A., Gimzewski, J.K., 2013. Nat. Commun. 4, 2811.
Robinson, J.T., Perkins, F.K., Snow, E.S., Wei, Z., Sheehan, P.E., 2008. Nano Lett. 8, 3137–3140.
Sato, T., Suzuki, Y., Mori., T., Maeda, M., Abe, M., Hino, O., Takahashi, K., 2014. Cancer Medicine 3, 1377–1384.
Song, L., Ci, L., Gao, W., Ajayan, P.M., 2009. ACS Nano 3, 1353–1356.
Shivaraman, S., Barton, R.A., Yu, X., Alden, J., Herman, L., Chandrashekhar, M.V.S., Park, J., McEuen, P.L., Parpia, J.M., Craighead, H.G., Spencer, M.G., 2009. Nano Lett. 9, 3100–3105.
Schwaedrle, M., Lazar, V., Validire, P., Hansson, J., Lacroix, L., Soria, J., Pawitan, Y., Kurzrock, R., 2015. Cancer Res. 75, 1187–1190.
Semeraro, F., Cancarini, A., Morescalchi, F., Romano, M.R., dell'Omo, R., Ruggeri, G., Agnifili, L., Costagliola, C., 2014. Diatetes Metab. 40, 445–451.
Teixeira, S., Burwell, B., Castaing, A., Gonzalez, D., Conlan, R.S., Guy, O.J., 2013. Sensor. Actuat. B-Chem. 190, 723–729.
Wang, H., Li, X., Mao, K., Li, Y., Du, B., Zhang, Y., Wei, Q., 2014. Anal. Biochem. 465, 121–126.
Xu, S., Man, B., Jiang, S., Yue, W., Yang, C., Liu, M., Chen, C., Zhang, C., 2014. Nanotechnology 25, 165702.
Yu, Q., Jauregui, L.A., Wu, W., Colby, R., Tian, J., Su, Z., Cao, H., Liu, Z., Pandey, D., Wei, D., Chung, T.F., Peng, P., Guisinger, N.P., Stach, E.A., Bao, J., Pei, S.S., Chen, Y.P., 2011. Nat. Mater. 10, 443–449.
Yue, W., Jiang, S., Xu, S., Bai, C., 2014. Biosens. Bioelectron. 195, 467–472.
Yang, J., Yang, F., Nie, J., Zou, X., Tian, H., Qin, Y., Liu, C., 2015. Cancer Biomark. 15, 211–217.
Yu, L., Shen, J., Mannoor, K., Guarnera, M., Jiang, F., Clin, 2014. Lung Cancer 15, 372.
Yasaei, P., Kumar, B., Hantehzadeh, R., Kayyalha, M., Baskin, A., Repnin, N., Wang, C., Klie, R.F., Chen, Y.P., Kral, P., Salehi-Khojin, A., 2014. Nat. Commun. 5, 1–8.
Yazyev, O., Louie, S.G., 2010. Nat. Mater. 9, 806–809.
Zhong, Z., Wu, W., Wang, D., Wang, D., Shan, J., Qing, Y., Zhang, Z., 2010. Biosens. Bioelectron. 25, 2379–2383.
Zhang, B., Li, Q., Cui, T., 2012. Biosens. Bioelectron. 31, 105–109.
Zheng, G., Patolsky, F., Cui, Y., Wang, W.U., Lieber, C.M., 2005. Nat. Biotechnol. 23, 1294–1301.
van der Zande, A.M., Barton, R.A., Alden, J.S., Ruiz-Vargas, C.S., Whitney, W., Pham, S., P. H, Q., Park, J., Parpia, J.M., Craighead, H.G., McEuen, P.L., 2010. Nano Lett. 10, 4869–4873.